# Quasicollapse of oblique solitons of the weakly dissipative derivative nonlinear Schrödinger equation

G. Sánchez-Arriaga

*Departamento de Física Aplicada, Escuela Técnica Superior de Ingenieros Aeronáuticos, Universidad Politécnica de Madrid, Plaza de Cardenal Cisneros 3, 28040 Madrid, Spain*

D. Laveder, T. Passot, and P. L. Sulem

*Université de Nice-Sophia Antipolis, CNRS, Observatoire de la Côte d'Azur, BP 4229, 06304 Nice Cedex 4, France*

Numerical integrations of the derivative nonlinear Schrödinger equation for Alfvén waves, supplemented by a weak dissipative term (originating from diffusion or Landau damping), with initial conditions in the form of a bright soliton with nonvanishing conditions at infinity (oblique soliton), reveal an interesting phenomenon of "quasicollapse": as the dissipation parameter is reduced, larger amplitudes are reached and smaller scales are created, but on an increasing time scale. This process involves an early bifurcation of the initial soliton toward a breather that is analyzed by means of a numerical inverse scattering technique. This evolution leads to the formation of persistent dark solitons that are only weakly affected when crossed by the decaying breather which has the form of either a localized structure or an extended wave packet.

## I. INTRODUCTION

The derivative nonlinear Schrödinger (NLS) equation,

$$\partial_t b + \partial_x[(|b|^2 - \langle|b|^2\rangle)b] + i\partial_{xx}b = 0, \qquad (1)$$

is obtained from the magnetohydrodynamic (MHD) equations with Hall effect (Hall-MHD) by means of a long-wavelength reductive perturbative expansion that isolates the dynamics of weakly nonlinear dispersive Alfvén waves propagating along a direction either parallel [1–3] or making a small angle [4,5] with the ambient magnetic field. In the former case, localized solutions are supposed to vanish at large distance and will be referred to as vanishing boundary condition (VBC) solutions. The latter one [referred to as nonvanishing boundary conditions (NVBCs)] corresponds to the nonzero boundary conditions $b(x,t) \to b_0$ at $\pm\infty$, where $b_0$ (that can be taken real) is the component of the ambient magnetic field perpendicular to the direction of propagation. It is also of interest to mention that the derivative nonlinear Schrödinger (DNLS) equation with such boundary conditions describes large amplitude MHD waves propagating at an arbitrary angle to the magnetic field in the limit of large $\beta$ [6]. The DNLS equation has been extensively used in the space physics literature to describe the dynamics of Alfvén waves that, as upstream of the earth's bow shock, propagate in directions making a relatively small angle with the ambient magnetic field and are associated with magnetic fluctuations whose amplitudes are large enough to make nonlinear couplings non-negligible (see, e.g., [7,8] and reference therein).

The fact that the DNLS equation governs the evolution of a complex field originates from the equality of the phase velocities of the parallel Alfvén and fast or slow (depending on $\beta$) magnetosonic waves in the zero dispersion limit. The solution $b = b_y + ib_z$ refers to the transverse magnetic field and $\langle\cdot\rangle$ denotes the average over the entire domain. For convenience, the equation has been rescaled in order to set the nonlinear and dispersive coefficients equal to unity. Furthermore, the mean value $\langle|b^2|\rangle$, which is a constant, can be eliminated by a change of frame.

For both vanishing and nonvanishing boundary conditions, the DNLS equation is completely integrable by inverse scattering transformation (IST) [9–12] and thus displays specific properties such as the existence of soliton solutions. It should in fact be viewed as an idealized model. In many physical instances, additional effects are indeed present that, albeit small, can significantly affect the dynamics. In particular, the question arises of the influence of a small dissipation on the soliton evolution [13]. In the Hall-MHD description of a collisional plasma, this effect can originate from Ohmic dissipation through a weak viscosity and/or magnetic diffusivity, leading to an additional term of the form $\mu\partial_{xx}b$ in the diffusive DNLS equation (see, e.g., [14] and references therein). In a noncollisional plasma, the dissipation originates from wave-particle resonance (Landau damping). In the latter case, a reductive perturbative expansion performed on the Vlasov-Maxwell equations leads to the so-called kinetic derivative nonlinear Schrödinger (KDNLS) equation [4,15–17],

$$\partial_t b + \partial_x[(1 - \sigma\mathcal{H})(|b|^2 - \langle|b|^2\rangle)b] + i\partial_{xx}b = 0, \qquad (2)$$

where

$$\mathcal{H}(|b|^2) = \frac{1}{\pi}\mathcal{P}\int_{-\infty}^{+\infty}\frac{|b|^2(x')}{x'-x}dx', \qquad (3)$$

and $\sigma$ is a small positive parameter that depends on the particle distribution and vanishes in the limit of cold plasmas. Other dissipative terms were also used in the literature aimed, for example, to simulate the ion-cyclotron damping [18]. As in the unperturbed problem, the term involving the mean value can be eliminated from dissipative DNLS equations by using a nonuniformly moving frame. It thus does not affect the dynamics but only shifts the structures spatially,

and so was suppressed in most of our simulations. Note that an alternative effect leading to a perturbed DNLS equation originates from homogeneous random fluctuations of the plasma density at equilibrium that leads to a nonlocal possibly negative linear diffusion [19].

Perturbative analyses based on the inverse scattering technique were developed to address the dynamics of soliton solutions of integrable equations, when a weak dissipative effect is retained [20,21]. The effect of a weak diffusion [22,23] or of Landau damping [24], on the so-called Alfvén soliton that is a parallel-propagating (i.e., VBC) solution, was in particular considered. In this approach, the solitonic character of the solution is to leading order preserved with an adiabatic evolution mostly due to variations of the soliton parameters (related to the associated eigenvalue) for which differential equations are derived and numerically integrated. The nonsoliton part of the solution, associated with radiation, was also considered and its relevance was evaluated in different regimes of parameters. Its spectral properties are in particular studied in [25], together with the space structure of the radiative field in the case of Ohmic dissipation. Deviations from the adiabatic theory were nevertheless observed in numerical integrations of the KDNLS equation [24] with an initial parallel-propagating soliton characterized by an eigenvalue with a positive real part, due to a significant distortion of the profile of the solution and an important radiation emission that can be captured in the framework of IST [25]. The inaccuracy of simple adiabatic modulation arguments for a soliton solutions of both the NLS and DNLS equations in the presence of a nonzero background that plays the role of an energy reservoir, was also discussed in the literature, and more systematic perturbation analyses were developed in the case of dark solitons [26–28]. The dynamics of NVBC bright solitons, considered in the present paper, is more difficult to address by the theory. The dynamics of NVBC solutions of the diffusive DNLS, initialized by a bright or dark soliton or by a breather, has recently been studied numerically [29], using an algorithm based on the inverse scattering technique (numerical IST) described in [30]. The formation of dark solitons as well as coalescence of bright and dark solitons to form a breather that eventually evolves toward a wave packet was reported. The former issue was in particular viewed by the authors as a possible mechanism at the origin of the magnetic depressions, usually referred to as magnetic holes, often observed in space plasmas.

In the present paper, we show that when the dissipation is small enough, the dynamics of a NVBC bright soliton leads to a kind of quasicollapse where, after becoming a breather, the solutions can locally reach a larger and larger amplitude and a smaller and smaller width as the dissipation coefficient is reduced, a process that nevertheless requires longer and longer times. Afterward, the soliton is rapidly dissipated with the generation of delocalized small-scale fluctuations. The paper is organized as follows. Section II provides a brief review of rigorous results concerning the DNLS equation, stressing their incomplete character. Section III provides explicit expressions for the DNLS solitons with NVBC, associated with real and complex eigenvalues. Section IV describes the results of numerical simulations of the DNLS equation with diffusion or Landau damping and points out

the destabilizing effect of a weak dissipation on the evolution of an initially bright NVBC soliton and the resulting formation of sharp structures. In Sec. V, the numerical IST is used to analyze in particular the coalescence of the bright soliton with an early created dark soliton, leading to a bifurcation to a breather whose amplitude, in contrast with that of bright solitons, is not bounded from above. Section VI provides a brief summary of our findings and includes in particular a few comments on the extensions of the present observations to the regime of strong dispersive turbulence that establishes when a random driving term is supplemented to the dissipative DNLS equation.

## II. BRIEF REVIEW OF RIGOROUS RESULTS

In the case of vanishing solutions at infinity, the equation (with no mean field) turns out to be equivalent, through a simple gaugelike transformation given in the case of zero condition at infinity by [23,31] $u(x,t) = b^*(x,t)\exp\frac{i}{2}\int_{-\infty}^{x}|b(\xi,t)|^2 d\xi$, to the equation

$$i\partial_t u + \partial_{xx} u + i|u|^2 \partial_x u = 0, \qquad (4)$$

that is written in terms of canonical variables relative to the Hamiltonian structure. An extension of this transformation to nonzero conditions at infinity or to periodic boundary conditions [32] is given in Appendix A. Equation (4) can be viewed as a special case of the so-called extended nonlinear Schrödinger equation that describes the evolution of the envelope of an ultrashort (typically femtosecond) nonlinear pulse propagating in an optical fiber, when the spectral width of the pulse is comparable with the carrier frequency [33,34]. In this regime, in addition to the usual Kerr nonlinearity, the effect of self-steepening of the pulse should indeed be taken into account. As usual in optics, the evolution variable $t$ then holds for the coordinate along the direction of propagation, while the variable $x$ refers to the delayed time associated with the group velocity of the pulse [35].

The DNLS equation possesses families of soliton solutions [36] that in the NVBC case include both bright and dark solitons (corresponding to real eigenvalues in the IST approach) and also breathers (for which the associated eigenvalue is complex). It is possible to define an infinity of conserved quantities that can easily be derived from those of Eq. (4) or its NVBC extension. The invariants associated with the symmetries of the DNLS equations for solutions with a limit $b_0$ at $\pm\infty$ are the energy $E = \int_{-\infty}^{+\infty}(|b|^2 - b_0^2)dx$, the momentum $P = \int_{-\infty}^{+\infty}[i(b\partial_x b^* - b^*\partial_x b) - (|b|^4 - b_0^4)]dx$, and the Hamiltonian $H = \int_{-\infty}^{+\infty}[|\partial_x b|^2 - \frac{i}{2}(\frac{3}{2}|b|^2 - b_0^2)(b\partial_x b^* - b^*\partial_x b) + \frac{1}{2}|b|^4(|b|^2 - b_0^2)]dx$. Such expressions are consistent with the invariants derived from the inverse scattering analysis (Eqs. (82)–(84) and (89) of [23]). An explicit recursive formula for computing the other invariants is given in [28]. Note that the presence of the fourth power term in the momentum is related to the fact that, in contrast with Eq. (4), the solution and its complex conjugate are not the canonical variables of Eq. (1) viewed as an Hamiltonian system (see Appendix A). An alternative formulation is discussed in [37] in the case of VBC solutions, where $P$ is viewed as a Hamiltonian either by dealing with a noncanonical Poisson bracket or by con-

sidering the magnetic field and the magnetic potential as conjugate canonical variables. A complete Hamiltonian formalism for NVBC solutions is developed in [38].

To this date, the mathematical theory of the DNLS equation remains incomplete. Existence in the large in time of Schwartz class solutions for a dense subset of initial conditions was reported, based on the analysis of the scattering and inverse scattering maps, which excludes certain "nongeneric" initial conditions characterized by specific spectral properties [39] (see also [40]). A direct proof of well posedness has only been given in the case of solutions vanishing at infinity with a small enough $L^2$ norm, typically $|b|_{L^2} < \sqrt{2\pi}$ (see [41,42] and reference therein). It is in this context interesting to note that the function $v(x,t) = b^*(x,t)\exp i\int_{-\infty}^x |b(\xi,t)|^2 d\xi$ obeys the usual quintic focusing nonlinear Schrödinger equation with an additional term $-iv^2\partial_x v^*$ that can counteract the focusing effect (see Appendix A). The existence of blowing up solutions remains an open problem, in spite of the existence of an infinite number of invariant quantities that do not necessary imply global smoothness. It is thus difficult to address rigorously the question of large-amplitude long-time behavior of solutions of the DNLS equation, and in particular their possible asymptotic evolution to a finite number of solitons supplemented by a radiation component, as in the case of the Korteweg–de Vries equation [43]. Nevertheless, orbital stability of solitonic solution vanishing at infinity was established in [44]. Furthermore, the structural stability of the real or complex eigenvalues associated with solitons of the DNLS equation in the NVBC case, relative to perturbations of the initial state, is studied in [45]. This reference also addressed the issue of the limiting regime where the imaginary part of the eigenvalue of a breather tends to zero, a question that is made delicate by the fact that a real eigenvalue can refer to either a bright or a dark soliton. The formation of solitonic structures in the case of oblique propagation is studied using the IST in [46,47]. The formation of solitons from a localized solution vanishing at infinity is analyzed in [48] and simulated numerically in [7]. Concerning the KDNLS equation, in spite of the (nonlinear) dissipation term associated with Landau damping, it is still unknown whether it admits classical solutions in the large-time limit. Only the existence of weak solutions was indeed established [49].

## III. OBLIQUE DNLS SOLITONS

The DNLS equation with NVBC admits two families of (oblique) solitons that are characterized by the eigenvalue $\lambda$ and the value at infinity $b_0$. For real $\lambda$, these solutions are commonly referred to as one-parameter (1P) solitons, and both dark and bright solitons are associated to a given value of $\lambda$. Solitons with complex $\lambda$ are called two-parameter (2P) solitons. They are breathers that, in a moving frame, are time periodic solutions. Recently, the IST analysis was reformulated using the affine parameter $\xi \equiv \gamma + i\beta$ defined by [12]

$$\lambda = b_0 \cosh \xi. \tag{5}$$

Using such a parameter simplifies the IST problem and provides a more compact expression of the solitons.

A 1P soliton is expressed as [24,50]

$$b = b_0 \left[ 1 - m \frac{2\left(1 - \frac{\eta}{\lambda}i\right)\exp(-z)}{\left[1 + m\frac{b_0^2}{2\eta^2}\left(1 - \frac{\eta}{\lambda}i\right)\exp(-z)\right]^2} \right], \tag{6}$$

where $\eta = \sqrt{b_0^2 - \lambda^2}$ and $z = 2\eta\lambda[x - (b_0^2 + 2\lambda^2)t]$. Here, $m = -1$ corresponds to a bright soliton and $m = +1$ corresponds to a dark one. Since, for $\gamma = 0$, the eigenvalue reads $\lambda = b_0 \cos \beta$, the 1P soliton is rewritten (up to a change in the origin of the space coordinate) as [12,23]

$$b(x,t) = b_0 \left[ 1 - \frac{2 \sin^2 \beta}{1 + m \cosh(z + i\beta)} \right], \tag{7}$$

where $z = k_0(x - V_0 t - x_0)$, with the soliton inverse width $k_0 = b_0^2 \sin 2\beta$ and the soliton velocity $V_0 = b_0^2(2 + \cos 2\beta)$. Here, $0 < \beta < \pi/2$ is related to the parameter $\beta_1$ used in [12,23] (that deals with a solution of an equation for $b^*$) by $\beta = \pi/2 - \beta_1$. The energy, momentum, and Hamiltonian of the soliton are easily calculated as [28,51] $E = 2\pi(1 - m) - 4\beta$, $P = 4b_0^2 \sin 2\beta$, and $H = -4b_0^4 \sin(4\beta)$. We note that the energy decays with the parameter $\beta$, and that

$$|b(x,t)|^2 = b_0^2[1 - 4 \sin^2 \beta f(z)], \tag{8}$$

with $f(z) = \cos \beta/(\cos \beta + m \cosh z)$. The maximum and minimum values of the bright and dark solitons are, respectively, given by $b_{max} = b_0(1 + 2 \cos \beta)$ and $b_{min} = b_0|1 - 2 \cos \beta|$. Further comments on the properties of this soliton are found in [23].

On the other hand, various analytical expressions have been given for DNLS 2P solitons. An expression was first reported in [51] (see also [50]), and in a factorized form in [29]. An independent derivation of a 2P soliton was made in [12] and was numerically checked to be equivalent to that given in [51]. It was in particular proved that it reproduces the 1P soliton when the eigenvalue becomes real and the VBC soliton as $b_0 \rightarrow 0$. In Appendix B, starting from Eq. (10) of [29], we show that the 2P soliton given in [51] can also be written in a form that, as in the case of the 1P soliton, separates the structure from the background, namely,

$$b = b_0 \left(1 + 4i \sinh 2\gamma \sin 2\beta \frac{Q}{R^2}\right), \tag{9}$$

where

$$Q = \sinh^2 \xi \cosh^2\left(\frac{\tilde{\phi}^* + \xi^*}{2}\right) - \sinh^2 \xi^* \cosh^2\left(\frac{\tilde{\phi} - \xi}{2}\right), \tag{10}$$

$$R = \sin 2\beta \sinh(\gamma - i\tilde{\phi}_i) + i \sinh 2\gamma \sinh(\tilde{\phi}_r - i\beta), \tag{11}$$

where $\tilde{\phi}$ is defined by the relation

$$\sinh 2\xi \sinh \xi e^{-i\phi} = i \frac{\sinh 2\gamma}{\sin 2\beta} e^{-\tilde{\phi}}, \qquad (12)$$

with $\phi = b_0^2 \sinh 2\xi [x - b_0^2(2 + \cosh 2\xi)t]$. This solution is periodic in time in the frame moving at the soliton velocity, with a period [12,23,51]

$$T = \frac{2\pi}{b_0^4 \tanh 2\gamma |\cos^2 2\beta - \cosh^2 2\gamma|}. \qquad (13)$$

The energy, momentum, and Hamiltonian of the 2P soliton are given by [12,23,51] $E = 4(\pi - 2\beta)$, $P = 8b_0^2 \sin(2\beta)\cosh(2\gamma)$, and $H = -2b_0^4 \cosh(4\gamma)\sin(4\beta)$.

## IV. EFFECT OF A WEAK DISSIPATION ON BRIGHT SOLITONS AND BREATHERS

We address in this section the effect of a weak Ohmic dissipation or of Landau damping on the evolution of an initial DNLS solitons in the NVBC case. For this purpose, numerical simulations were performed using a spectral code in a periodic domain whose extension $L = 50\pi$ (or in some instances, such as in Fig. 9, $100\pi$) is much larger than the width of the soliton. Such a large domain is required in order to reduce as much as possible the influence of the spatial periodicity. Due to the cubic character of the DNLS equation, aliasing was eliminated by computing the nonlinear term with a number of collocation points that is twice larger than the effective resolution specified in the following for each simulation. The time stepping is made using a (fully explicit) third-order Runge-Kutta scheme with a time step four times smaller than prescribed by the stability condition in order to accurately resolve all the retained scales. In all the simulations with NVBC solitons as initial conditions, we used $b_0 = 1$, and varied the associated eigenvalue and the dissipation coefficient.

Figure 1 displays the time evolution of an initial bright 1P soliton with $\lambda = 0.975$, when the DNLS equation is perturbed by an Ohmic dissipation with a diffusivity $\mu = 10^{-5}$. A resolution of $2^{15} = 32\,768$ effective mesh points was used for this simulation. In spite of the small value of the diffusion coefficient, dissipation produces a dramatic effect on the dynamics, leading in particular to a strong amplification of the amplitude (here by a factor of order 4.5) and a significant reduction in the soliton width. As discussed below, we refer to this evolution as a quasicollapse that is followed by a relaxation process where the soliton reverses its direction of propagation, with a significant energy radiation. With the aim of analyzing more quantitatively the influence of the dissipation on the dynamics, simulations were performed with different values $\mu = 10^{-3}$, $10^{-4}$, and $10^{-5}$ of the diffusion coefficient. Figure 2 (top) displays the maximum amplitude $M$ of the solution versus time for each of these runs. One observes that increasingly large maximum amplitudes are obtained when the diffusivity $\mu$ is reduced, albeit after a longer and longer time. In order to quantify the time evolution of the typical smallest scales, we show in Fig. 2 (middle) the instantaneous logarithmic decrement $\delta$ obtained by fitting the energy spectrum $|\hat{b}_y(k)|^2 + |\hat{b}_z(k)|^2$ of the solution by a func-
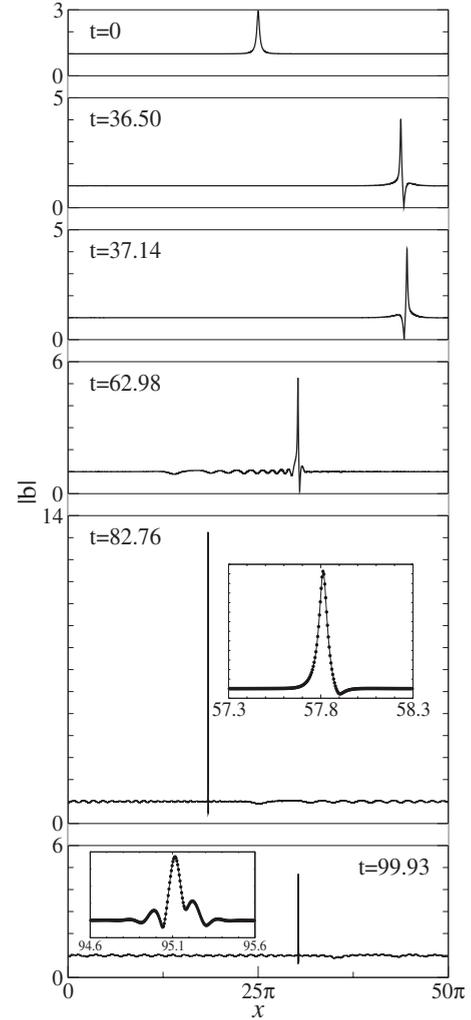


FIG. 1. Time evolution of an initial bright soliton with eigenvalue $\lambda = 0.975$, as prescribed by the diffusive DNLS equation with $\mu = 10^{-5}$. The insets (where the mesh points are displayed) provide details of the solution near the soliton at the corresponding times.

tion $ck^{2\alpha}e^{-2\delta k}$ [52]. The fact that the minimum value reached by $\delta$ decreases with $\mu$ indicates the formation of smaller and smaller scales as the diffusion coefficient is reduced. The accuracy of the simulation is ensured by the observation that, even at its minimum, the logarithmic decrement $\delta$ remains larger than several mesh sizes. During the whole period of accurate fit, the algebraic prefactor $\alpha$ remains equal to 1 with a rather good accuracy. It is noticeable that up to a time that is very close to the quasicollapse, the product $\delta M^2$ remains almost constant, a property consistent with the scale invariance of the nondissipative DNLS equation. The same scaling holds for the quintic one-dimensional nonlinear Schrödinger equation that in the focusing cases leads a finite-time blowup. Extrapolation of these observations suggests a singular behavior of the solution of the dissipative DNLS equation when taking the double limit $\mu \to 0$ together with $t \to \infty$ with a specific scaling that the few available data suggest to be $t \sim \mu^{-0.7}$. A similar evolution is observed when the Ohmic dissipation is replaced with Landau damping, as shown in Fig. 3 that corresponds to integrations of the KDNLS equation with the same initial 1P soliton (associated
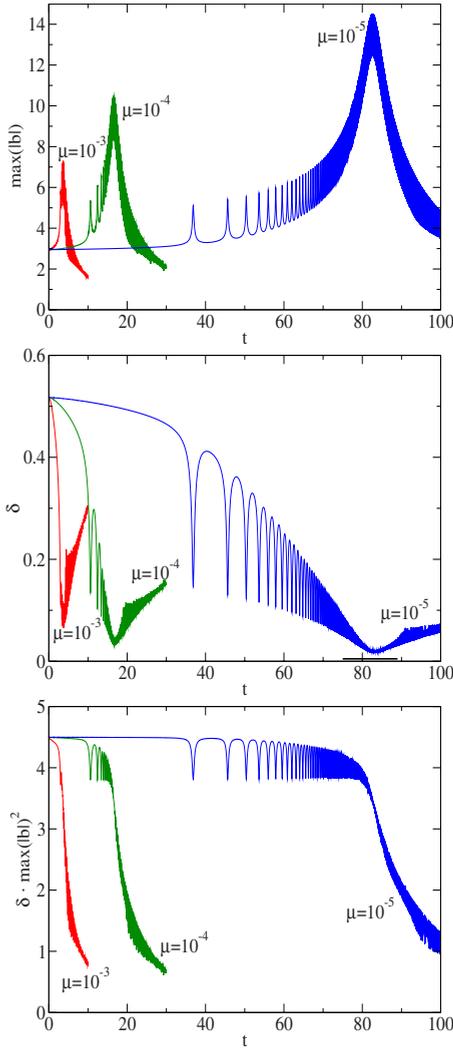
FIG. 2. (Color online) Time evolution of the maximal amplitude $M$ (top) of the logarithmic decrement $\delta$ (middle), with the mesh size indicated by a thick black line, and of the product $M\delta^2$ (bottom), for an initial bright soliton with $\lambda=0.975$, evolving according to the diffusive DNLS equation with $\mu=10^{-3}$ (red line), $10^{-4}$ (green line) and $10^{-5}$ (blue line).



FIG. 3. (Color online) Time evolution of the maximal amplitude $M$, the logarithmic decrement $\delta$, and the product $M\delta^2$ of an initial bright soliton with $\lambda=0.975$, evolving according to KDNLS equation with $\sigma=10^{-3}$ (red line) and $10^{-4}$ (green line).

with $\lambda=0.975$) as in Fig. 2, and $\sigma=10^{-3}$ and $10^{-4}$.

In order to address the influence of dissipation on quantities that are invariants of the unperturbed DNLS equation, we plot in Fig. 4 the time variation of the energy $E$ (top), the momentum $P$ (middle), and the Hamiltonian $H$ (bottom) for the diffusive DNLS equation in the same conditions as in Fig. 2 (initial 1P soliton with $\lambda=0.975$ and three values $\mu=10^{-3}$, $10^{-4}$, and $10^{-5}$ of the diffusivity). After an early period whose duration is longer as $\mu$ is decreased and during which the energy is only weakly dissipated, we observe a sharp decay of $E$ (Fig. 4, top) at the moment when the soliton profile starts developing significant small scales. After the latter has been dissipated, the energy variation becomes much milder. The inflection point of the curve $E(t)$ roughly corresponds to the maximum of the momentum $P$ that, in this case, has then been amplified by a factor of 200. As $P$ grows, the Hamiltonian first becomes strongly negative, reaching a value close to $-1.43\times10^3$, before rapidly growing

to a very high positive value (larger than $4.52\times10^3$) at a time close to the second inflection point of $P(t)$. Similar but significantly softer variations are observed with larger values of $\mu$. As shown in Fig. 5 (top), the energy dissipation $2\mu\int|\partial_x b|^2 dx$ at a given time tends to zero with $\mu$, and so does its maximum. Nevertheless, since smaller and smaller scales are formed as $\mu$ is decreased, the maximum of $\int|\partial_x b|^2 dx$ (that occurs at increasing times) grows in a "quasisingular" way in this limit (Fig. 5, bottom).

The question then arises of the influence of the initial conditions, as characterized by the soliton eigenvalue $\lambda$, on the observed dynamics. When considering initial 1P bright solitons associated with (real) values of $\lambda$ decreasing from the maximal value $\lambda=1$, the dynamics tends to be slightly less violent and much slower. For example, as $\lambda$ is reduced from $\lambda=0.975$ to 0.7 and 0.2 with $\mu=10^{-4}$, the maximal value reached by the amplitude decreases from 10.5 to 10.0 and 9.7, respectively. The associated times are 16.6, 67.7, and 6132. In order to discuss the influence of initial condi-
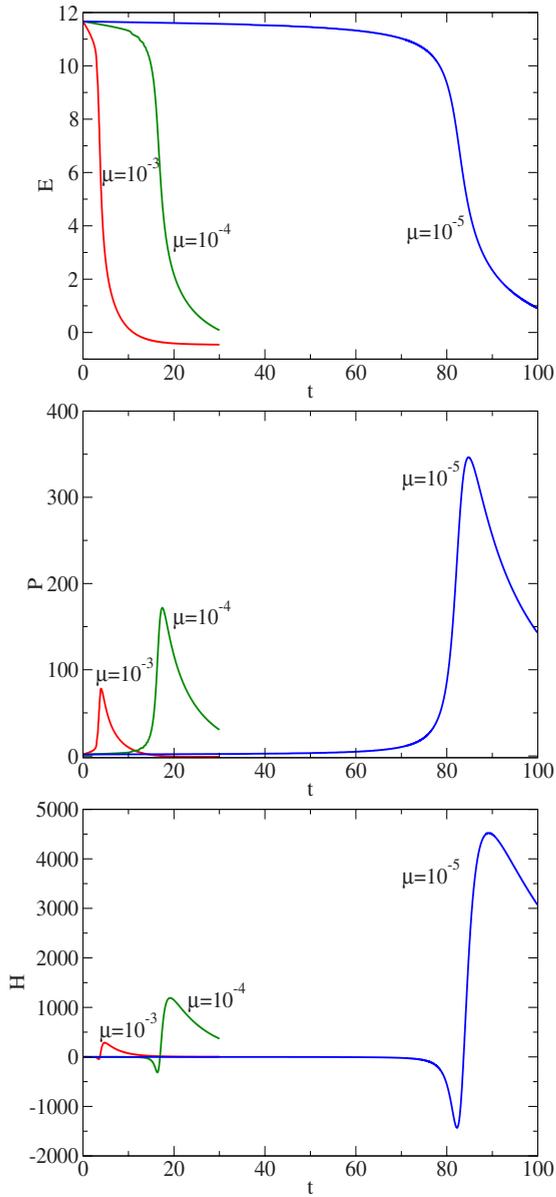
FIG. 4. (Color online) Time evolution of the energy $E$ (top), the momentum $P$ (middle), and the Hamiltonian $H$ (bottom) for the dissipative DNLS equation with diffusion coefficients $\mu = 10^{-3}$ (red line), $\mu = 10^{-4}$ (green line), and $\mu = 10^{-5}$ (blue line), in the case of an initial bright NVBC soliton associated with an eigenvalue $\lambda = 0.975$.

tions in the form of a 2P soliton corresponding to complex values of $\lambda = \lambda_r + i\lambda_i$ with increasing imaginary parts, we performed simulations with $\lambda_r = 0.7$ and $\lambda_i = 0$, 0.01, 0.05, 0.2, 0.25, and 0.35. Figure 6 displays for different values of $\mu$ the maximum amplitude of the solution versus $\lambda_i$. We observe that within the explored ranges of parameters, increasing $\lambda_i$ leads to a decrease in the maximum. For larger $\lambda_i$, the sensitivity of this maximum to the value of the coefficient $\mu$ decreases. For $\lambda_i = 0.25$, the values of the maxima essentially coincide in the cases $\mu = 10^{-5}$ and $\mu = 10^{-6}$, while for $\lambda_i = 0.35$, it is already the case with $\mu = 10^{-4}$ and $\mu = 10^{-5}$. The instants of these maxima scale like $1/\mu$. This result is exemplified in Fig. 7 that, for $\lambda_i = 0.35$, displays the time variation
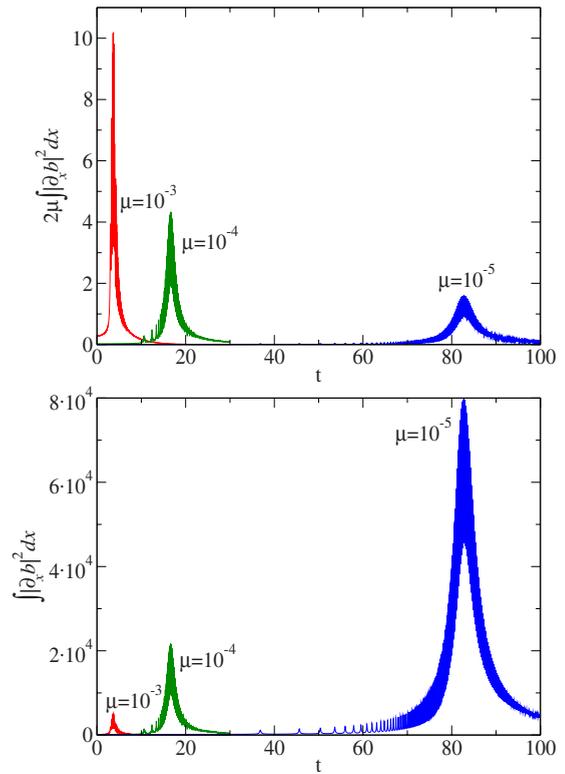


FIG. 5. (Color online) Time evolution of the energy dissipation (top) and of the integral norm of the square solution gradient (bottom), in the conditions of Fig. 4.

of instantaneous maximum of the solution amplitude versus $\mu t$ for $\mu = 10^{-4}$ and $\mu = 10^{-5}$, both during the entire simulation (top) and during a shorter time interval near the absolute maximum. The latter panel reveals that, if the envelopes of the curves corresponding to the two values of $\mu$ superimpose accurately, the breather oscillation periods are significantly different, scaling approximately like $1/\mu^2$.

In order to study the sensitivity of the long-time profile of the solution to the initial conditions and to the diffusivity, we
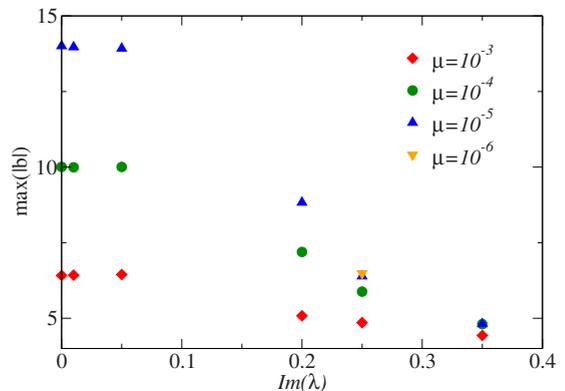


FIG. 6. (Color online) Maximum amplitudes of the solution of the dissipative DNLS equation obtained from an initial bright NVBC soliton with $b_0 = 1$ and an eigenvalue $\lambda$ such that Re$(\lambda) = 0.7$ and Im$(\lambda) = 0$, 0.01, 0.05, 0.2, 0.25, and 0.35, and various diffusion coefficients $\mu = 10^{-3}$ (red diamonds), $10^{-4}$ (green circles), $10^{-5}$ (blue triangles), and for Im$(\lambda) = 0.25$, $\mu = 10^{-6}$ (yellow inverted triangle).
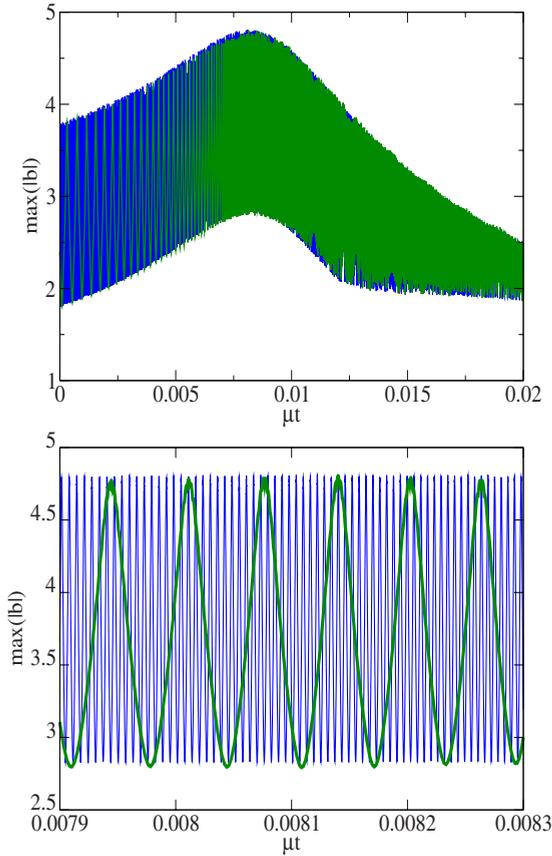
FIG. 7. (Color online) Instantaneous maximal amplitude of the solution of dissipative DNLS equation versus $\mu t$ for initial conditions corresponding to a 2P soliton with $\lambda = 0.7 + 0.35i$ and two diffusion coefficients. The slower oscillation (green line) corresponds to $\mu = 10^{-4}$ and the faster one (blue line) corresponds to $\mu = 10^{-5}$. The top panel refers to the whole simulation and the bottom one provides an enlargement near the absolute maximum of the amplitude.

plot in Fig. 8 snapshots of the solution profile for $\lambda = 0.7$ (left), $\lambda = 0.7 + 0.05i$ (middle), and $\lambda = 0.7 + 0.35i$ (right), for diffusivities $\mu = 10^{-3}$ (top) and $10^{-4}$ (bottom), after approximately two crossings of the entire domain. We observe the formation of magnetic holes that are quasistatic, in agreement with [29]. The soliton travels rapidly across them without creating permanent deformations and is progressively transformed into a wave packet. Both the formation of the persistent magnetic holes and the transition toward a wave packet that is eventually dissipated are favored when the viscosity is not too small and the value of $\lambda_i$ is moderate.

Figure 9 provides an example of a 2P initial soliton (with an eigenvalue $\lambda = 0.5 + 0.1i$) that for $\mu = 10^{-5}$ breaks into a dark and a bright soliton. The dark soliton appears to be stable while the bright one displays a quasicollapse. The time evolution of its maximum amplitude is shown in Fig. 10. Superimposed is the amplitude of a VBC soliton ($b_0 = 0$) with the same initial eigenvalue for diffusivities $\mu = 10^{-5}$ and $10^{-4}$ (blue and green lines, respectively). The dynamics of the VBC is very mild, indicating that the phenomenon of quasicollapse requires nonzero boundary conditions. Furthermore, the two latter curves superimpose accurately, when plotted versus $\mu t$, indicating a trivial scaling.

## V. BIFURCATION TOWARD A QUASICOLLAPSING 2P SOLITON

The fact that the amplitude of a bright 1P soliton is bounded from above suggests that an effect of a weak dissipation is to induce a bifurcation of such an initial condition toward a 2P soliton that is not subject to such a constraint. To analyze this point more specifically, the associated eigenvalues are to be evaluated. A tool based on the IST theory was developed in [30] to analyze nonlinear dispersive waves corresponding to either observational data or to solutions of numerical simulations by evaluating eigenvalues associated
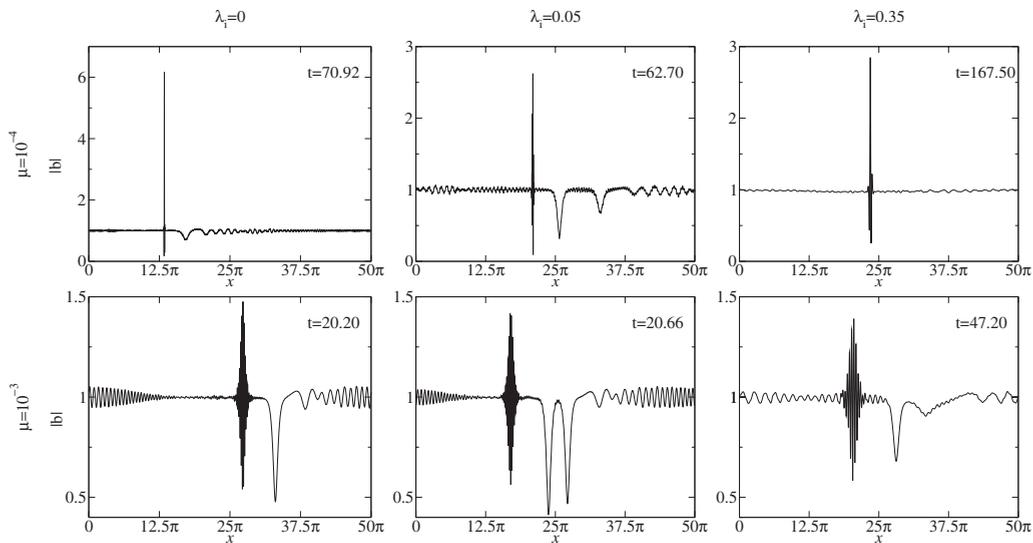


FIG. 8. Snapshots of the solution profile in the case of an initial bright NVBC soliton with $\lambda_i = 0$ (left), 0.05 (middle), and 0.35 (right), for $\mu = 10^{-4}$ (top) and $\mu = 10^{-3}$ (bottom), at different times given, from left to right and top to bottom, by $t = 70.92$, 62.70, 167.50, 20.20, 20.66, and 47.20.
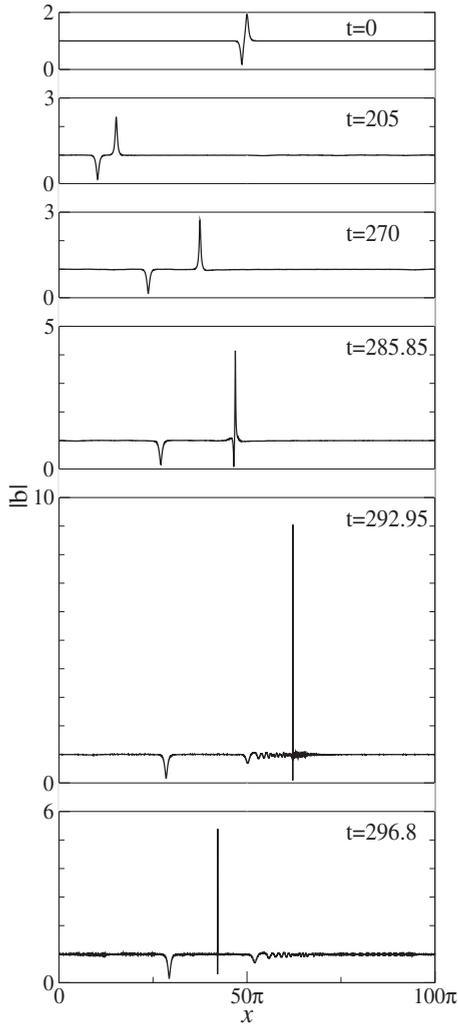
FIG. 9. Time evolution of an initial 2P soliton with eigenvalue $\lambda=0.5+0.1i$ and $b_0=1$, as prescribed by the diffusive DNLS equation with $\mu=10^{-5}$. Note that at the last displayed instant of time (bottom panel), the soliton has reversed its direction of propagation.

with embedded solitonic structures, and was exemplified in the case of the DNLS equation with vanishing boundary conditions.

Without presenting a comprehensive discussion of the IST that is well documented in the literature, we briefly sketch here the main ideas of the method and of its numerical implementation. A first step in the IST approach consists of writing the dynamical equation (here, the DNLS equation) as the solvability condition for a system of two linear equations for a $(2 \times 2)$ matrix $\Phi$ of the form

$$\Phi_x = D\Phi, \tag{14}$$

$$\Phi_t = F\Phi, \tag{15}$$

where $D$ and $F$ are matrices whose coefficients are explicitly given in terms of a time-independent parameter $\lambda$ and of the solution $b(x,t)$. Given the nonvanishing boundary conditions at infinity, one defines two solutions $\Phi^+$ and $\Phi^-$ of Eqs. (14) and (15), satisfying the boundary conditions at $+\infty$ and $-\infty$,
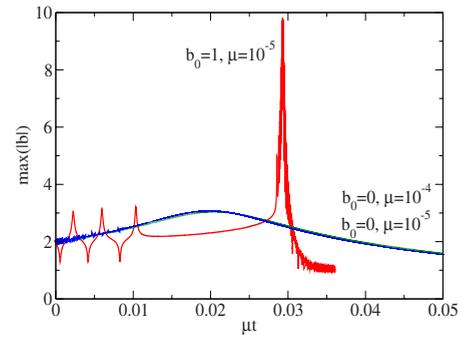


FIG. 10. (Color online) Variation versus $\mu t$ of the maximal amplitude of the diffusive DNLS equation for initial conditions in the form of initial NVBC soliton with eigenvalue $\lambda=0.5+0.1i$, when $\mu=10^{-5}$ (red line), and of a VBC soliton with the same eigenvalue, in the cases $\mu=10^{-5}$ (blue line) and $\mu=10^{-4}$ (green line). The curves corresponding to the VBC solitons with different $\mu$'s superimposed exactly, up to a time rescaling.

respectively. These two solutions are related by

$$\Phi^- = \Phi^+ S, \tag{16}$$

where $S$ is the scattering matrix. As detailed in [29] where a self-contained description of the method is presented, boundedness requires that the element $S_{11}$ of the scattering matrix vanishes. The isolated values of $\lambda$ obeying this condition are called the eigenvalues and are associated with a soliton of the dynamical equation. The numerical IST consists essentially of computing these eigenvalues by means of a Newton-Raphson method where the iteration is initialized by the values of the eigenvalues at the previous time. In the cases where the solitons are clearly separated in physical space, the analysis is performed on a suitable restriction of the computational domain.

This approach was used in [29] to analyze the results of a direct numerical simulation of the DNLS equation supplemented with an additional Ohmic term, using a 1P or a 2P oblique soliton as initial condition. In this section, we use the numerical IST for a partial analysis of the simulations we have performed. We first addressed the early time dynamics of a bright DNLS soliton and its bifurcation to a 2P soliton, focusing on the influence of the diffusion coefficient on this process. As already mentioned, such a transition is a prerequisite for a quasicollapse dynamics. For this purpose, we used as initial condition a NVBC soliton corresponding to an eigenvalue $\lambda=0.7$, and various diffusivities $\mu=10^{-3}$, $10^{-4}$, and $10^{-5}$. Figure 11 displays the variations of these eigenvalues versus the rescaled time $\mu t$ for the above diffusion coefficients. A main issue is that at early times, two real eigenvalues are detected: one originating from the initial soliton and a second one obtained by initiating the eigenvalue computation algorithm with the value $\lambda=1$ (more generally, $\lambda=b_0$). This indicates that the dissipative term leads the solution to rapidly become a multisoliton solution (a third real eigenvalue is detected when $\mu=10^{-4}$ and $\mu=10^{-5}$). Explicit forms of NVBC two-soliton solutions of the DNLS equation are given in [53], and extension to $N$ solitons is discussed in [23]. Note that the eigenvalue associated with the bright soli-
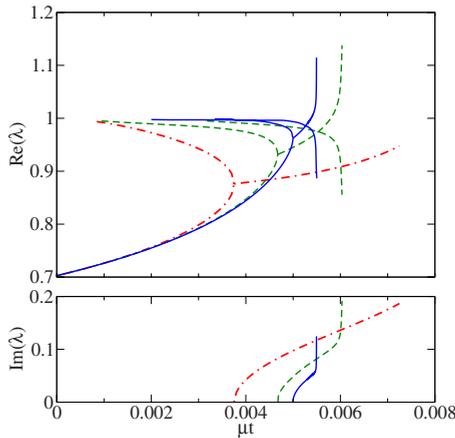
FIG. 11. (Color online) IST analysis of solutions of dissipative DNLS equation with initial conditions corresponding to a bright soliton with $\lambda = 0.7$, for various values of the diffusion coefficients $\mu = 10^{-3}$ (red dashed-dotted line), $10^{-4}$ (green dashed line), and $10^{-5}$ (blue solid line). The real (top panel) and imaginary (bottom panel) parts of the eigenvalues are plotted versus the rescaled time $\mu t$.

ton increases during the evolution and this leads to a growth of the soliton energy. The creation of a dark soliton is thus necessary to ensure that the energy of the full solution (whose energy, when it is composed of 1P solitons, is the sum of the corresponding energies) decreases in time [54]. At later times, we observe the collision of the two real eigenvalues, leading a bifurcation to a 2P soliton (breather) that can evolve to a sharp structure. Furthermore, when comparing the graphs associated with the different values of $\mu$, we note that while at early times changing this parameter reduces to a time rescaling, the moment where the soliton eigenvalue becomes complex occurs later than suggested by this rescaling. This in particular leads the real eigenvalue to reach larger values before the bifurcation takes place, which enables the bifurcated solution to develop a stiffer behavior.

The additional eigenvalues correspond to dark solitons that are difficult to observe in physical space at early time, not only because of their small amplitudes but also because they can only be created in the regions of large gradients and thus cannot be easily separated from the bright soliton. They nevertheless play an important role as the collision of a bright and a dark soliton is necessary for the formation of a breather. The number of dark solitons formed before the bifurcation is difficult to estimate, but it is clear that a dark soliton with eigenvalue $\lambda = 1$ (and thus a zero amplitude and infinite scale) should appear as soon as dissipation is turned on. In other words, the 1P bright soliton immediately becomes a two-soliton solution [53] and possibly later on a multisoliton solution [23]. In fact, a simple modulation argument obtained by plugging a 1P bright soliton in the equation for the energy variation is inconsistent with the energy decay under the effect of dissipation, while dealing with a two-soliton solution (a bright and a dark one), and plugging its expression in the equations for the variations of $E$ and $P$ leads to an evolution consistent with a monotonic energy decay.

The predictions of the numerical IST are validated by comparing the solution obtained by direct numerical simula-
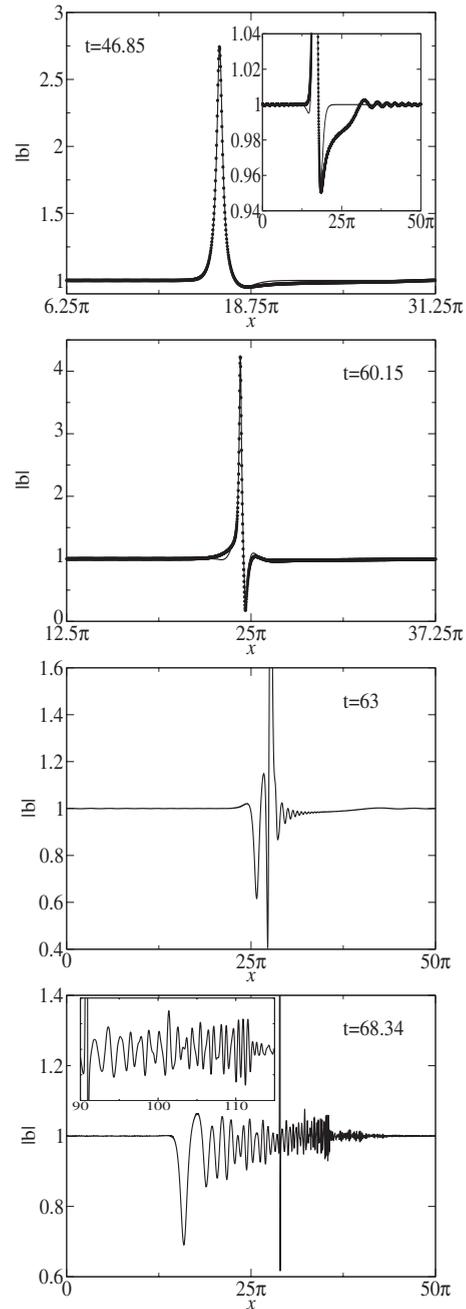


FIG. 12. Simulation in the conditions of Fig. 11, when $\mu = 10^{-4}$. From top to bottom: solution profile at the eigenvalue bifurcation time $t = 46.85$ (dots) and 2P soliton (solid line) reconstructed by means of numerical IST, together with (in the inset) a detail showing that a local correction is expected from the additional real eigenvalue and from the radiation; similar comparison at the last time ($t = 60.15$) of the IST implementation; solution profile when a complicated structure starts developing ($t = 63$); *idem* when, after passing the amplitude maximum at $t = 67.8$, the soliton starts moving backward ($t = 68.34$), with the inset displaying emitted radiation.

tion with the soliton reconstructed from the IST computed eigenvalue. The top panel ($t = 46.85$) in Fig. 12 displays, in the case $\mu = 10^{-4}$, the solution at the instant of the bifurcation in the region of significant variations, together with the soliton reconstructed from the complex eigenvalue (thus neglect-

ing the influence of the detected real eigenvalue). Note that since the profile of the 2P soliton evolves periodically in time, it had to be selected at a suitable stage of its evolution to perform the fit. We observe a satisfactory agreement, with the maximum and minimum of the amplitude being in particular well reproduced. The inset nevertheless shows that, as expected, the profile of the actual solution is locally affected by the real eigenvalue (associated with a dark soliton) and also by the continuous spectrum leading to the radiation visible on the graph. The panel at $t=60.15$ provides a comparison between the numerical solution and the soliton associated with the complex eigenvalue, at the end of the IST analysis. The agreement is again satisfactory. The further evolution is however difficult to analyze using IST due to the complexity of the solution. The panel at time $t=63$ corresponds to the moment when the solution begins to develop a richer structure. The amplitude maximum is reached at $t \approx 67.8$. At $t=68.34$, the numerically computed soliton changes its propagation direction and starts moving backward (bottom panel). Strong radiation is then emitted by the soliton, leading to the formation of disorganized small-scale structures whose details are displayed in the inset.

The long-time evolution of the solutions is easier to analyze with numerical IST when the system is more dissipative. In order to illustrate such a regime that is closer to those addressed in [29] (with Ohmic dissipation instead of Landau damping), we considered the KDNLS equation with an initial 1P soliton corresponding to $\beta=0.6$ (or $\lambda \approx 0.825$), using a parameter $\sigma=0.01$. Figure 13 (top) shows the evolution of the amplitude maximum as obtained by direct integration of Eq. (1). In order to analyze the dynamics of the scattering data, Fig. 13 (bottom) shows the evolution of the eigenvalues as calculated with the numerical IST. At early times, the eigenvalue increases from its initial value $\lambda=0.825$, which is consistent with the enhancement of the amplitude. As in the previous simulations, another real eigenvalue originating from $\lambda=1$ is rapidly visible. After the coalescence of these two eigenvalues at $t \approx 0.53$, the resulting complex eigenvalue can be followed during a rather long time. We note by $t=3.32$ the appearance of an additional real eigenvalue. The accuracy of the analysis up to the end of the simulation is supported by Fig. 14 that displays at $t=6.00$, the profile of the numerical solution, and a reconstruction based on the complex and real eigenvalues evaluated by the numerical IST. The agreement is rather good up to the radiation that is not retained in the present IST analysis and leads to oscillations of the solution profile on the right-hand side of the dark soliton.

## VI. CONCLUSION

We have studied numerically the evolution of an oblique DNLS soliton subject to a weak dissipation in the form of either diffusion (viscosity and/or Ohmic dissipation) or Landau damping. In the case where the initial condition is a bright soliton, we confirm the early transition to a breather [29], as the result of the coalescence with a dark soliton created by the dissipative perturbation. The immediate formation of at least one dark soliton (magnetic hole) is essen-
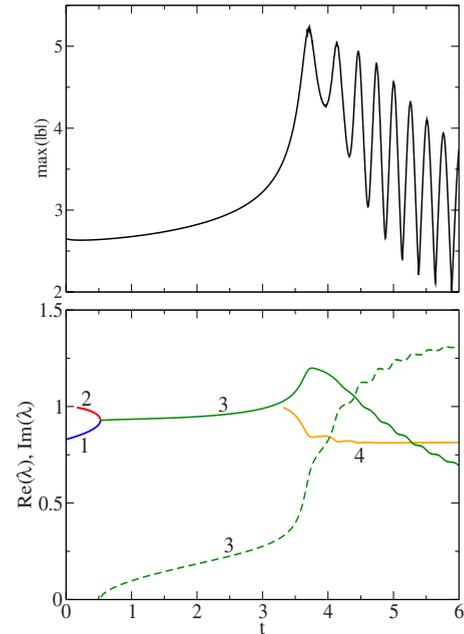


FIG. 13. (Color online) Top: time variation of the maximal amplitude of the solution of the KDNLS equation with $\sigma=0.01$ and an initial bright soliton characterized by $b_0=1$ and $\lambda=0.825$; bottom: IST analysis of this solution. Label (1) corresponds to the initial 1P bright soliton, (2) to the early formed dark soliton, (3) to the bifurcated 2P soliton, and (4) to a second dark soliton. Solid lines correspond to real eigenvalues or to the real part of the complex one, while the dashed line refers to its imaginary part.

tial for consistency with energy decay. A main observation concerns the influence of reducing the diffusion or the Landau damping coefficient. It turns out that the solution then reaches increasingly large amplitudes and develops smaller and smaller scales, on a time scale that also becomes longer and longer. This picture suggests an asymptotic wave collapse when the double limit of decreasing dissipation and increasing times (with the suitable scaling) is taken. Further theoretical developments are required for getting a detailed understanding of this quasicollapse.
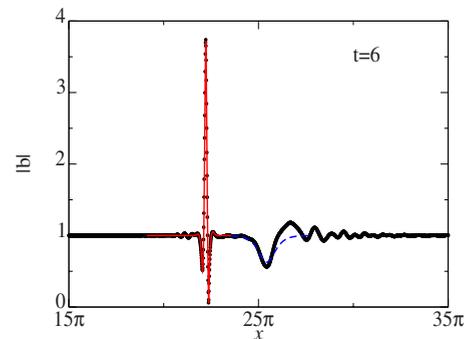


FIG. 14. (Color online) Snapshot at time $t=6$ of the solution profile (dark dots) of the KDNLS equation in the conditions of Fig. 13, with superimposed 2P soliton (solid red line) and the dark soliton (dashed blue line) reconstructed from the computed eigenvalues, $\lambda=0.6944+1.3171i$ and $\lambda=8.814$. Note that due to the high density of mesh points, the dark dots look like a thick line outside the 2P soliton.

We note that the DNLS equation displays common features, such as the scaling properties, with the quintic (i.e., critical in one space dimension) NLS equation that can develop a finite-time singularity. Simple qualitative arguments concerning the effect of radiation on the contribution to the invariants originating from a region of negative Hamiltonian, which were successfully applied to the NLS equations or some of its extensions [55–57], might thus suggest the possibility of a wave collapse for the DNLS equation after a finite or an infinite time. A main difference between DNLS and the critical NLS equations nevertheless originates from the complete integrability of the former equation that in particular prescribes the existence of an infinite number of invariants.

As already mentioned, a simple gauge transformation changes the DNLS equation into a focusing quintic NLS equation, but with an additional term that is expected to prevent blowup. Nevertheless, since the effect of dissipation is stronger on higher-order invariants, one may think that in the presence of viscosity, the constraints originating from the integrability are depleted, permitting the solution to develop a quasisingular dynamics that is then arrested by the dissipation enhancement due to the resulting small-scale formation. The soliton is indeed rapidly damped after reaching the amplitude maximum.

It is of interest to mention that similar sharp bright solitonic structures are also spontaneously formed (together with dark or wave-packet solitons) in the turbulent regime that develops when the dissipative DNLS equation is subject to a large-scale random driving which is a white noise in time [58]. The process discussed in the present paper (and in particular the generation of small-scale incoherent oscillations visible, for example, in Fig. 12, bottom) thus appears to be a robust phenomenon playing a main role in the strongly intermittent small-scale energy transfer that develops in the regime of strong dispersive turbulence. It should nevertheless be mentioned that the precise conditions for the generation of bright oblique solitons remain essentially open due to the various possible profiles of 2P solitons. Indeed, while an initial isolated magnetic hole rapidly evolves toward a train of dark solitons [50,59], the evolution of an oblique magnetic hump rather leads to solitons with the form of wave packets. Further studies are required to characterize the long-time evolution of general DNLS solutions, depending on the initial data.

The question then arises of the possible relevance of the above findings for space plasmas. Clearly, the DNLS equation that only retains the competition between wave steepening and dispersion (here, in the presence of a weak dissipation) is an oversimplified model to address the highly complicated dynamics of media such as the solar wind or planet magnetosheaths. Nevertheless, since this model is not limited to quasiparallel propagation but remains valid in oblique or quasitransverse directions when the ion beta is large enough, a possible connection between the formation of dark solitons, as the result of the action of a weak dissipation on early formed bright solitons, and magnetic depressions (holes) commonly observed in the interplanetary medium (see, for example, [60] and references therein) was recently discussed [29]. In this context, it is of interest to note that

direct numerical simulations of the one-dimensional Hall-MHD equation along an oblique direction subject to an external driving show in some instances the formation of bright solitonic structures that survive collisions and preserve their coherence on several time units [61]. This contrasts with DNLS VBC solitons that were reported to be unstable approximations of solutions of the parallel Hall-MHD equations, in that they evolve relatively rapidly and dissipate [62].

## APPENDIX A: VARIOUS FORMS OF THE DNLS EQUATION

Starting from Eq. (1) without the mean term $\langle |b|^2 \rangle$, and defining $\psi = b^*$, we obtain the DNLS equation in the form of how it arises in nonlinear optics,

$$i\partial_t \psi + \partial_{xx}\psi + i\partial_x(|\psi|^2\psi) = 0. \tag{A1}$$

Writing $\psi = Ae^{i\varphi}$, where the amplitude $A$ and the phase $\varphi$ are real, we get

$$A_t + 2A_x\varphi_x + A\varphi_{xx} + 3A^2A_x = 0, \tag{A2}$$

$$A\varphi_t - A_{xx} + A\varphi_x^2 + A^3\varphi_x = 0. \tag{A3}$$

Let us now define $\widetilde{\varphi}$ such that

$$\widetilde{\varphi}_x = \varphi_x + \alpha(A^2 - A_0^2), \tag{A4}$$

where $\alpha$ is a real parameter. In the case of nonzero boundary conditions $A_0 = \lim_{\pm\infty}|\psi|$, while in the case of periodic boundary conditions, $A_0 = \sqrt{\langle |\psi|^2 \rangle}$, where the angular brackets indicate spatial averaging on the periodic domain. It follows from Eq. (A4) that

$$\varphi_t = \widetilde{\varphi}_t + 2\alpha A^2\widetilde{\varphi}_x + \alpha\left(\tfrac{3}{2} - 2\alpha\right)(A^4 - A_0^4) + 2\alpha^2 A_0^2(A^2 - A_0^2), \tag{A5}$$

where the integration constant ensures that the phase is constant at infinity when dealing with an infinite domain or keeps a mean zero value when the domain is periodic. As a consequence, we obtain

$$A_t + 2A_x\widetilde{\varphi}_x + A\widetilde{\varphi}_{xx} + (3 - 4\alpha)A^2A_x + 2\alpha A_0^2 A_x = 0, \tag{A6}$$

$$A\widetilde{\varphi}_t - A_{xx} + A\widetilde{\varphi}_x^2 + A^3\widetilde{\varphi}_x + 2\alpha A_0^2 A\widetilde{\varphi}_x$$
$$+ \alpha A(A^2 - A_0^2)\left[\left(\tfrac{1}{2} - \alpha\right)A^2 + \left(\tfrac{3}{2} - \alpha\right)A_0^2\right] = 0. \tag{A7}$$

The complex amplitude $u = Ae^{i\widetilde{\varphi}}$ then satisfies

$$iu_t + u_{xx} + 2i(1 - \alpha)|u|^2u_x$$
$$+ (1 - 2\alpha)\left[iu^2u_x^* - \frac{\alpha}{2}|u|^2(|u|^2 - A_0^2)u\right]$$
$$- \alpha\left(\frac{3}{2} - \alpha\right)A_0^2(|u|^2 - A_0^2)u = 0, \tag{A8}$$

where the additional term $2i\alpha A_0^2 u_x$ has been suppressed by a Galilean transformation. Furthermore, the definition of $\widetilde{\varphi}$ depends on the boundary conditions.

For solutions vanishing at infinity,

$$\widetilde{\varphi} = \varphi + \alpha \int_{-\infty}^{x} A^2(x')dx'. \qquad (A9)$$

For solutions with a finite amplitude $A_0$ at both $\pm\infty$,

$$\widetilde{\varphi} = \varphi + \alpha \int_{-\infty}^{x} [A^2(x') - A_0^2]dx'. \qquad (A10)$$

For periodic boundary conditions [32],

$$\widetilde{\varphi} = \varphi + \alpha \left\langle \int_{\theta}^{x} [A^2(x') - \langle A^2 \rangle]dx' \right\rangle_{\theta}, \qquad (A11)$$

where the subscript $\theta$ specifies that the spatial averaging is done relative to the lower bound $\theta$ of the integral. Note that in the case of nonzero conditions at infinity, $\lim_{x\to-\infty} u = A_0$, while $\lim_{x\to+\infty} u = A_0 \exp(i\alpha E)$, where $E$ is the energy.

Two special cases are of special interest:

(i) For $\alpha = 1/2$, the equation has a canonical form relative to the Hamiltonian structure, in the sense that it can be rewritten as

$$i\frac{\partial u}{\partial t} = \frac{\delta \mathcal{H}}{\delta u^*}, \qquad (A12)$$

$$i\frac{\partial u^*}{\partial t} = -\frac{\delta \mathcal{H}}{\delta u}, \qquad (A13)$$

for the Hamiltonian

$$\mathcal{H} = \int \Bigg[ |u_x|^2 + \frac{i}{4}(u_x^* u - u_x u^*)|u|^2 + \frac{A_0^2}{4}|u|^2(|u|^2 - A_0^2)$$
$$- \frac{A_0^4}{4}(|u|^2 - A_0^2) \Bigg] dx. \qquad (A14)$$

In this representation, the momentum takes the simple form

$$\mathcal{P} = \frac{i}{2} \int (u_x^* u - u_x u^*)dx. \qquad (A15)$$

Going back to the variable $b$, it reproduces the momentum of the DNLS equation given in the Introduction. The Hamiltonian $\mathcal{H}$ reduces to $H$ up to an additional term $-(b_0^4/4)\int(|b|^2 - b_0^2)dx$ that is proportional to the energy $E$.

It is of interest to note that in the case of zero boundary conditions at infinity, the equation reduces to

$$iu_t + u_{xx} + i|u|^2 u_x = 0, \qquad (A16)$$

which implies

$$\partial_t |u|^2 + \partial_x \Big[ i(u_x^* u - u_x u^*) + \frac{1}{2}|u|^4 \Big] = 0. \qquad (A17)$$

One also has

$$i\partial_t \int_{-\infty}^{+\infty} x(u_x^* u - u_x u^*)dx = 4\mathcal{H}. \qquad (A18)$$

Nevertheless, in contrast with the critical NLS equation (see, e.g., [63] for a review), the density of energy current $i(u_x^* u - u_x u^*) + \frac{1}{2}|u|^4$ differs from the momentum density. This prevents, in the case of the DNLS equation, the establishment of a variance identity (which is a main ingredient in proving wave collapse for critical NLS equation). The absence of such an identity reflects the noninvariance of the equation by pseudoconformal transformation.

(ii) For $\alpha = 1$, one has, when assuming for the sake of simplicity zero boundary conditions at infinity,

$$iu_t + u_{xx} + \frac{1}{2}|u|^4 u - iu^2 u_x^* = 0 \qquad (A19)$$

that differs from the focusing quintic NLS equation (that can lead to a finite-time blowup of the solution) by the last term in the left-hand side. It is still not proved that this term prevents the solution to collapse, but numerical simulations strongly suggest that it does so.

## APPENDIX B: 2P SOLITON

Writing the complex eigenvalue $\lambda = b_0 \cosh \xi$, with $\xi = \gamma + i\beta$, the expression for the 2P soliton given in Eq. (10) of [29] rewrites in the form $b = b_0(1 + \frac{N}{D})$, with

$$N = mnf^*g^* - f^2g^2 + (1+k)(2fg - f^*g^* - mn), \qquad (B1)$$

$$D = [fg - (1+k)]^2, \qquad (B2)$$

where

$$m = 1 + \frac{\sinh 2\xi \sinh \xi}{(\cosh \xi - \sinh \xi)^3}e^{-i\phi}, \qquad (B3)$$

$$n = 1 + \frac{\sinh 2\xi^* \sinh \xi^*}{(\cosh \xi^* + \sinh \xi^*)^3}e^{i\phi^*}, \qquad (B4)$$

$$f = 1 + \frac{\sinh 2\xi \sinh \xi}{\cosh \xi - \sinh \xi}e^{-i\phi}, \qquad (B5)$$

$$g = 1 + \frac{\sinh 2\xi^* \sinh \xi^*}{\cosh \xi^* + \sinh \xi^*}e^{i\phi^*}, \qquad (B6)$$

$$k = \frac{\sinh^2 2\gamma}{\sin^2 2\beta}, \qquad (B7)$$

$$\phi = b_0^2 \sinh 2\xi[x - b_0^2(2 + \cosh 2\xi)t]. \qquad (B8)$$

It is convenient to define the variable $\widetilde{\phi}$ by the relation

$$\sinh 2\xi \sinh \xi e^{-i\phi} = i\frac{\sinh 2\gamma}{\sin 2\beta}e^{-\widetilde{\phi}}. \qquad (B9)$$

The above formulas become

$$m = 1 + i\frac{\sinh 2\gamma}{\sin 2\beta}e^{-\widetilde{\phi}+3i\beta+3\gamma}, \qquad (B10)$$

$$n = 1 - i\frac{\sinh 2\gamma}{\sin 2\beta}e^{-\tilde{\phi}^*+3i\beta-3\gamma}, \tag{B11}$$

$$f = 1 + i\frac{\sinh 2\gamma}{\sin 2\beta}e^{-\tilde{\phi}+i\beta+\gamma}, \tag{B12}$$

$$g = 1 - i\frac{\sinh 2\gamma}{\sin 2\beta}e^{-\tilde{\phi}^*+i\beta-\gamma}. \tag{B13}$$

In the denominator,

$$fg - (1+k) = 2i\frac{\sinh 2\gamma}{\sin^2 2\beta}e^{-\tilde{\phi}_r+i\beta}[\sin 2\beta\,\sinh(\gamma - i\tilde{\phi}_i)$$

$$+ i\,\sinh 2\gamma\,\sinh(\tilde{\phi}_r - i\beta)]. \tag{B14}$$

In the numerator

$$fg = 1 + 2\frac{i\sinh 2\gamma}{\sin 2\beta}\sinh(\gamma - i\tilde{\phi}_i)e^{-\tilde{\phi}_r+i\beta} + \left[\frac{\sinh 2\gamma}{\sin 2\beta}e^{-\tilde{\phi}_r+i\beta}\right]^2, \tag{B15}$$

$$mn = 1 + 2i\frac{\sinh 2\gamma}{\sin 2\beta}\sinh(3\gamma - i\tilde{\phi}_i)e^{-\tilde{\phi}_r+3i\beta}$$

$$+ \left[\frac{\sinh 2\gamma}{\sin 2\beta}e^{-\tilde{\phi}_r+3i\beta}\right]^2. \tag{B16}$$

It follows that

$$2fg - f^*g^* - mn = 4i\frac{\sinh 2\gamma}{\sin 2\beta}e^{-\tilde{\phi}_r+i\beta}[\sinh^2 \xi^* e^{-\gamma+i\tilde{\phi}_i}$$

$$- \sinh^2 \xi e^{\gamma-i\tilde{\phi}_i}] + 4[\sinh 2\gamma e^{-\tilde{\phi}_r+i\beta}]^2. \tag{B17}$$

Furthermore, defining $X = (\sinh 2\gamma/\sin 2\beta)e^{-\tilde{\phi}_r+i\beta}$, one has

$$f^2g^2 = 1 + 4iX\sinh(\gamma - i\tilde{\phi}_i) + 2X^2[2 - \cosh(2\gamma - 2i\tilde{\phi}_i)]$$

$$+ 4iX^3\sinh(\gamma - i\tilde{\phi}_i) + X^4, \tag{B18}$$

$$mnf^*g^* = 1 + 2iX(\cosh 2\xi e^{\gamma-i\tilde{\phi}_i} - \cosh 2\xi^* e^{-\gamma+i\tilde{\phi}_i})$$

$$+ 2X^2[\cosh 4i\beta + \cosh 4\gamma - \cosh(2\gamma - 2i\tilde{\phi}_i)]$$

$$+ 2iX^3(\cosh 2\xi^* e^{\gamma-i\tilde{\phi}_i} - \cosh 2\xi e^{-\gamma+i\tilde{\phi}_i}) + X^4. \tag{B19}$$

We note that

$$mnf^*g^* - f^2g^2 = 4iX(\sinh^2 \xi e^{\gamma-i\tilde{\phi}_i} - \sinh^2 \xi^* e^{-\gamma+i\tilde{\phi}_i})$$

$$+ 4X^2(\sinh^2 2\gamma - \sin^2 2\beta)$$

$$+ 4iX^3(\sinh^2 \xi^* e^{\gamma-i\tilde{\phi}_i} - \sinh^2 \xi e^{-\gamma+i\tilde{\phi}_i}), \tag{B20}$$

and the numerator reads

$$N = -8i\left(\frac{\sinh 2\gamma}{\sin 2\beta}\right)^3 e^{-2\tilde{\phi}_r+2i\beta}[\sinh^2 \xi\,\cosh(\tilde{\phi}^* + \xi^*)$$

$$- \sinh^2 \xi^*\,\cosh(\tilde{\phi} - \xi) + i\,\sinh 2\gamma\,\sin 2\beta]. \tag{B21}$$

One finally gets the 2P NVBC soliton in the form announced in Sec. II,

$$b = b_0\left(1 + 4i\,\sinh 2\gamma\,\sin 2\beta\frac{Q}{R^2}\right), \tag{B22}$$

with

$$Q = \frac{1}{2}[\sinh^2 \xi\,\cosh(\tilde{\phi}^* + \xi^*) - \sinh^2 \xi^*\,\cosh(\tilde{\phi} - \xi)$$

$$+ i\,\sinh 2\gamma\,\sin 2\beta] = \sinh^2 \xi\,\cosh^2\left(\frac{\tilde{\phi}^* + \xi^*}{2}\right)$$

$$- \sinh^2 \xi^*\,\cosh^2\left(\frac{\tilde{\phi} - \xi}{2}\right), \tag{B23}$$

$$R = \sin 2\beta\,\sinh(\gamma - i\tilde{\phi}_i) + i\,\sinh 2\gamma\,\sinh(\tilde{\phi}_r - i\beta). \tag{B24}$$

[1] K. Mio, T. Ogino, K. Minami, and S. Takeda, J. Phys. Soc. Jpn. **41**, 265 (1976).
[2] E. Mjølhus, J. Plasma Phys. **16**, 321 (1976).
[3] E. Mjølhus, J. Plasma Phys. **19**, 437 (1978).
[4] E. Mjølhus and J. Wyller, J. Plasma Phys. **40**, 299 (1988).
[5] C. F. Kennel, B. Buti, T. Hada, and R. Pellat, Phys. Fluids **31**, 1949 (1988).
[6] M. S. Ruderman, J. Plasma Phys. **67**, 271 (2002).
[7] S. Spangler, in *Nonlinear Waves and Chaos in Space Plasmas*, edited by T. Hada and H. Matsumoto (Terra Scientific Publishing Company, TERRAPUB, Tokyo, 1997), pp. 171–224.
[8] B. Buti, V. L. Galinski, V. I. Shevchenko, G. S. Lakhina, B. T. Tsurutani, B. E. Goldstein, P. Diamond, and M. V. Medvedev, Astrophys. J. **523**, 849 (1999).
[9] D. Kaup and A. Newell, J. Math. Phys. **19**, 798 (1978).
[10] V. S. Gerdzhikov, M. I. Ivanov, and P. P. Kulish, Theor. Math. Phys. **44**, 784 (1980).
[11] T. Kawata and H. Inoue, J. Phys. Soc. Jpn. **44**, 1968 (1978).
[12] X. J. Chen and W. K. Lam, Phys. Rev. E **69**, 066604 (2004).
[13] Y. S. Kivshar and B. A. Malomed, Rev. Mod. Phys. **61**, 763 (1989).
[14] C. Wu and C. F. Kennel, J. Plasma Phys. **47**, 85 (1992).
[15] A. Rogister, Phys. Fluids **14**, 2733 (1971).
[16] E. Mjølhus and J. Wyller, Phys. Scr. **33**, 442 (1986).
[17] T. Passot and P. L. Sulem, Phys. Plasmas **10**, 3887 (2003).
[18] S. R. Spangler, Phys. Fluids **29**, 2535 (1986).
[19] M. Ruderman, Phys. Plasmas **9**, 2940 (2002).
[20] V. I. Karpman and E. M. Maslov, Sov. Phys. JETP **46**, 281

(1977).; **48**, 252 (1978).

[21] D. J. Kaup and A. C. Newell, Proc. R. Soc. London, Ser. A **361**, 413 (1978).

[22] J. Wyller and E. Mjølhus, Physica D **13**, 234 (1984).

[23] V. M. Lashkin, J. Phys. A **40**, 6119 (2007).

[24] J. Wyller, T. Flå, and E. Mjølhus, Physica D **39**, 405 (1989).

[25] V. Lashkin, Phys. Rev. E **74**, 016603 (2006).

[26] S. Burtsev and R. Camassa, J. Opt. Soc. Am. B **14**, 1782 (1997).

[27] X. J. Chen, Z. D. Chen, and N. N. Huang, J. Phys. A **31**, 6929 (1998).

[28] X. J. Chen, L. J. Hou, and W. K. Lam, Chin. Phys. Lett. **22**, 830 (2005).

[29] R. L. Hamilton, D. A. Peterson, and S. M. Libby, J. Geophys. Res. **114**, A03104 (2009).

[30] T. Hada, R. L. Hamilton, and C. F. Kennel, Geophys. Res. Lett. **20**, 779 (1993).

[31] Y. H. Ichikawa, K. Konno, M. Wadati, and H. Sanuki, J. Phys. Soc. Jpn. **48**, 279 (1980).

[32] S. Herr, Int. Math. Res. Notices **2006**, 96763 (2006).

[33] N. Tzoar and M. Jain, Phys. Rev. A **23**, 1266 (1981).

[34] D. Anderson and M. Lisak, Phys. Rev. A **27**, 1393 (1983).

[35] A. Newell and J. Moloney, *Nonlinear Optics* (Addison-Wesley, Reading, MA, 1992).

[36] T. Hada, C. F. Kennel, and B. Buti, J. Geophys. Res. **94**, 65 (1989).

[37] S. P. Dawson and C. F. Fontán, J. Plasma Phys. **40**, 585 (1988).

[38] H. Cai and N.-N. Huang, J. Phys. A **39**, 5007 (2006).

[39] J. H. Lee, Trans. Am. Math. Soc. **314**, 107 (1989).

[40] J. C. DiFranco and P. D. Miller, Physica D **237**, 947 (2008).

[41] N. Hayashi and T. Ozawa, Physica D **55**, 14 (1992).

[42] J. Colliander, M. Keel, G. Staffilani, H. Takaoka, and T. Tao, SIAM J. Math. Anal. **33**, 649 (2001).

[43] W. Eckhaus and P. Schuur, Math. Methods Appl. Sci. **5**, 97 (1983).

[44] M. Colin and M. Ohta, Ann. Inst. Henri Poincare, Anal. Non Lineaire **23**, 753 (2006).

[45] R. L. Hamilton, C. F. Kennel, and E. Mjølhus, Phys. Scr. **46**, 230 (1992).

[46] R. L. Hamilton, C. F. Kennel, and E. Mjølhus, Phys. Scr. **46**, 237 (1992).

[47] V. M. Lashkin, Phys. Rev. E **71**, 066613 (2005).

[48] Y. H. Ichikawa and Y. Abe, Prog. Theor. Phys. **94**, 128 (1988).

[49] D. Rial, Nonlin. Anal. **49**, 149 (2002).

[50] E. Mjølhus and T. Hada, in *Nonlinear Waves and Chaos in Space Plasmas*, edited by T. Hada and H. Matsumoto (Terra Scientific Publishing Company, TERRAPUB, Tokyo, 1997), pp. 121–169.

[51] E. Mjølhus, Phys. Scr. **40**, 227 (1989).

[52] C. Sulem, P. L. Sulem, and H. Frisch, J. Comput. Phys. **50**, 138 (1983).

[53] X.-J. Chen, H.-L. Wang, and W. K. Lam, Phys. Lett. A **353**, 185 (2006).

[54] G. Sánchez-Arriaga (unpublished).

[55] V. E. Zakharov, Sov. Phys. JETP **35**, 908 (1972).

[56] E. A. Kuznetsov, Chaos **6**, 381 (1996).

[57] D. Agafontsev, F. Dias, and E. Kuznetsov, JETP Lett. **87**, 667 (2008).

[58] D. Laveder, T. Passot, P. L. Sulem, and G. Sánchez-Arriaga (unpublished).

[59] D. Laveder, D. Borgogno, T. Passot, and P. L. Sulem, Comput. Phys. Commun. **180**, 1860 (2009).

[60] B. Buti and B. E. Goldstein, Adv. Space Res. **32**, 291 (2003).

[61] D. Laveder, L. Marradi, T. Passot, and P. L. Sulem, Planet. Space Sci. (to be published).

[62] B. Buti V. Jayanti A. F. Vi nas, S. Ghosh, M. L. Goldstein, D. A. Roberts, G. Lakhina, and B. T. Tsurutani, Geophys. Res. Lett. **25**, 2377 (1998).

[63] C. Sulem and P.-L. Sulem, *The Nonlinear Schrödinger Equation: Self-Focusing and Wave Collapse*, Applied Mathematical Sciences No. 139 (Springer, New York, 1999).